CRACK PATH STABILITY IN TAPERED DCB SPECIMENS

Y. Sumi*

Based on the concept of intermediate range of crack path stability proposed by the present author, investigations are made for crack path stability in tapered double cantilever beam (DCB) specimens. The present stability theory is an extension of the concept proposed by Cotterell and Rice, and includes not only the crack tip local stability parameter so called T-stress but also another parameter which represents the effect of the change of the stability along the curved trajectory. Numerical computations are performed to obtain the stability parameters, and the present fracture criterion is verified by experiments, where specimens made of PMMA are quasi-statically fractured under displacement controlled conditions.

INTRODUCTION

It has recently been recognized that crack paths sometimes play essential roles in obtaining the precise evaluation of the entire fracture process to the final breakoff of solids by brittle cracking. Several criteria have been proposed for the crack branching angles under the mixed mode loading conditions. A sharply curved crack extension is, however, observed by Radon et al. [1] for a predominantly Mode I tensile crack, where biaxial tension exists at the crack tip. Cotterell and Rice [2] examined the problem and proposed the T-stress theory, in which they introduced the concept of crack path stability. Sumi, Nemat-Nasser, and Keer [3] extended the concept to an intermediate range of stability, which may be applicable to a much wider range of problems such as crack curving due to severe bending at the crack tip.

In the present paper investigations are made for the crack path stability of variously tapered DCB specimens by the stability parameters derived from the proposed theory, and by experiments which provide various stable and unstable paths of brittle cracking.

* Faculty of Engineering, Yokohama National University
Tokiwadai, Hodogaya-ku, Yokohama 240, Japan

INTERMEDIATE RANGE OF STABILITY FOR THE CRACK PATH

Fig.1 shows a straight crack with slightly branched and curved extension, where V indicates the domain of the body, and surface tractions, t_i, and surface displacements v_i are prescribed on the boundaries $S_t+S_c^{\pm}$ and S_u, respectively. The Cartesian coordinate system (x_1,x_2) is introduced with the origin at the tip, and the slightly branched and curved extension, whose surfaces are denoted by $S_b^{\pm}$, has its projected length, h, on the x_1-axis. The stress state ahead of the original crack tip is given by

$$\sigma_{11}(x_1,0) = \frac{k_I}{\sqrt{2\pi x_1}} + T + b_I\sqrt{\frac{x_1}{2\pi}} + O(x_1), \tag{1}$$

$$\sigma_{22}(x_1,0) = \frac{k_I}{\sqrt{2\pi x_1}} + b_I\sqrt{\frac{x_1}{2\pi}} + O(x_1), \tag{2}$$

$$\sigma_{12}(x_1,0) = \frac{k_{II}}{\sqrt{2\pi x_1}} + b_{II}\sqrt{\frac{x_1}{2\pi}} + O(x_1), \tag{3}$$

where k_I and k_{II} are the stress intensity factors at the original crack tip, and the coefficients T, b_I, b_{II} are also determined from the solution of the boundary value problem prior to the crack extension. The curved crack profile is assumed to have the following form:

$$\lambda(x_1) = \alpha x_1 + \beta x_1^{3/2} + \gamma x_1^{2} + O(x_1^{5/2}), \tag{4}$$

where α, β, and γ are the shape parameters.

Stress Intensity Factors at the Extended Crack Tip

As was given by Sumi [4], stress intensity factors at the branched and curved extension are represented as

$$K_I = (k_I - \frac{3}{2}\alpha k_{II}) - \frac{9}{4}\beta k_{II} h^{1/2} + \{\frac{b_I}{2} - \frac{5}{4}\alpha b_{II} - 3\gamma k_{II} + k_I\bar{k}_{11} - \alpha k_I(\bar{k}_{12} + \frac{3}{2}\bar{k}_{21}) + k_{II}\bar{k}_{12} - \alpha k_{II}(\bar{k}_{11} + \frac{3}{2}\bar{k}_{22})\}h, \tag{5}$$

$$K_{II} = (k_{II} + \frac{1}{2}\alpha k_I) + (\frac{3}{4}\beta k_I - 2\sqrt{\frac{2}{\pi}}\alpha T)h^{1/2} + \{\frac{b_{II}}{2} - \frac{\alpha}{4}b_I - \frac{3\sqrt{2\pi}}{4}\beta T + \gamma k_I + k_I\bar{k}_{21} + \alpha k_I(\frac{1}{2}\bar{k}_{11} - \bar{k}_{22}) + k_{II}\bar{k}_{22} + \alpha k_{II}(\frac{1}{2}\bar{k}_{12} - \bar{k}_{21})\}h. \tag{6}$$

The quantities $\bar{k}_{1j}$ and $\bar{k}_{2j}$ (j=1,2) are the stress intensity factors of Mode I and Mode II of the following problems, where the cases for j=1 and 2 correspond respectively to the ones for μ=I and II;

$$\sigma_{ij,j} = 0 \qquad \text{in } V,$$

$$\sigma_{ij} n_j = -\sigma^{f}_{\mu ij} n_j \qquad \text{on } S_t + S_c^{\pm},$$

$$u_i = -u^{f}_{\mu i} \qquad \text{on } S_u \qquad \mu = \text{I, II.} \tag{7}$$

Stresses σ^{f}_{Iij} and σ^{f}_{IIij} are respectively the fundamental stress fields of Mode I and Mode II defined by Bueckner [5], and u^{f}_{Ii} and u^{f}_{IIi} are the corresponding displacement fields.

The crack path can be obtained by using the locally symmetric deformation ahead of the crack tip, which is expressed as

$$K_{II} = 0, \tag{8}$$

along the curved trajectory. This condition leads to the following shape parameters;

$$\alpha = -2k_{II}/k_I, \tag{9}$$

$$\beta = \frac{8}{3}\sqrt{\frac{2}{\pi}}\,(T/k_I)\alpha\,, \tag{10}$$

$$\gamma = -\left(k_{II}\bar{k}_{22} + k_I\bar{k}_{21} + \frac{b_{II}}{2}\right)\frac{1}{k_I} + \left[\left\{k_I(2\bar{k}_{22} - \bar{k}_{11}) + \frac{b_I}{2}\right\}\frac{1}{2k_I} + 4(T/k_I)^2\right]\alpha. \tag{11}$$

Intermediate Range of Crack Path Stability

We consider the case, where noncolinear crack growth is caused by some disturbance introduced in the system with a small, initial kink angle α at the original crack tip, which is the imperfection parameter of the system. The crack path stability is then examined by taking account of the second and third terms of Eqn.(4). As can be seen from Eqn.(11), the first three terms of γ represent the smooth curving of the crack path without imperfection. This crack path may be considered as the fundamental path with $k_{II} = 0$. The effect of crack path stability appeared in γ is the rest of the terms given in Eqn.(11). The crack path stability is determined from the quantity D_s, expressed as

$$D_s \equiv (\beta^*/\alpha) + (\gamma^*/\alpha)\sqrt{h/L_s} \begin{cases} < 0\text{: stable} \\ > 0\text{: unstable,} \end{cases} \tag{12}$$

where β^* and γ^* are nondimensionalized by a representative length L_s of the body and given by

$$\beta^*/\alpha = \frac{8}{3}\sqrt{\frac{2}{\pi}}\,(T/k_I)L_s^{1/2}, \tag{13}$$

$$\gamma^*/\alpha = [\{k_I(2\bar{k}_{22} - \bar{k}_{11}) + \frac{b_I}{2}\}\frac{1}{2k_I} + 4(T/k_I)^2]L_s\,. \tag{14}$$

Crack path stability for Mode I loading conditions can be determined from the values of β^*/α and γ^*/α, which are expressed in terms of k_I, T, b_I, $\bar{k}_{11}$, and $\bar{k}_{22}$.

CRACK PATH STABILITY IN TAPERED DCB SPECIMENS

Fracture testing can effectively be performed, if it is possible to find out an appropiate geometry of the specimen which provides relatively long crack propagation in comparison with its size. DCB specimens are typical examples of the specimens which satisfy such a requirement. Crack paths in DCB specimens are, however, observed to be unstable in experiments (for example see Ref.[3]), which show sharp crack curving and the final breakoff of the specimen may occur at either the upper or lower surface of the specimen. Since it has been experienced that crack paths are to a certain extent stabilized by using tapered DCB specimens, their crack path stabilities are examined by numerical calculations and experiments. Fig.2 shows three types of rectangular fracture specimens, whose length L is varied for Type-A, Type-BM, and Type-BL specimens. Three tapered DCB specimens are shown in Fig.3, where the taper angles are changed for Type-CN, Type-CM, and Type-CW specimens.

Crack Path Stability Examined by Numerical Calculations

Calculations are made for the stability parameters β^*/α and γ^*/α of the crack paths given by Eqns.(13) and (14) for various crack lengths of the specimens, where the stress field parameters at the crack tip are calculated by the method of superposition of analytical and finite-element solutions (Yamamoto, Tokuda, and Sumi [6,7]). These numerical results are shown in Fig.4 and Fig.5, where the representative length L_s is taken as $L_s = B$.

Having obtained the above numerical results, crack path stability can be examined by Eqn.(12), where we consider the crack growth length being within the range $h/L_s \leqq 0.4$ and $h/H \leqq 0.1$ in order to ensure the validity of the first order perturbation analysis.

We have $\beta^*/\alpha > 0$ and $\gamma^*/\alpha < 0$ for A-specimen, where the locally unstable crack path is stabilized in the intermediate range. We can, therefore, expect a stable crack path. Since the effect of bending appears for BM-specimen, we have $\beta^*/\alpha > 0$, and $\gamma^*/\alpha > 0$ for $0.3 < H/L < 0.7$. A crack path might become unstable when the crack tip extends to the middle part of the specimen. This tendency is rather significant for BL-specimens, where we have $\beta^*/\alpha > 0$ and $\gamma^*/\alpha > 0$. Crack paths become unstable for this specimen.

A slightly tapered geometry is introduced in CN-specimen, but the stability parameters indicate almost the same unstable tendency as those of BL-specimen. The stabilizing effect of the tapered geometry begins to appear in CM-specimen, where we have $\beta^*/\alpha > 0$, and $\gamma^*/\alpha < 0$ for H/L>0.65. Crack paths are still unstable when the crack tip extends to the middle part of the specimen. A significant stabilizing effect is expected for the CW-specimen, where the stability parameters are $\beta^*/\alpha > 0$, and $\gamma^*/\alpha < 0$ except for the small range around H/L=0.5.

Experimental Results and Discussions

Actual crack paths are obtained by experiments for the six types of specimens made of PMMA material. The initial notch lengths are 45mm for CW-specimens and 60mm for the rest of the specimens, respectively. Natural fracture surfaces, whose lengths are a few millimeters, are formed by wedge forces applied to the notch roots. Test specimens are then loaded by pins through pin holes under the displacement controlled condition, and it is observed that the crack growth behaviour is almost quasi-static during the entire fracture process.

The experimentally measured crack paths are shown from Fig.6 to Fig.11, where the scale of Fig.6 is enlarged ten times in the virtical direction and the rest of the figures are similarly scaled down from the actual specimens. As can be seen from these figures, crack paths are unstable for BL and CN-specimens and the crack directions are sharply turned towards either the upper or lower surface of the specimens. In contrast, crack paths are stable for A, BM, and CW-specimens, while both stable and unstable crack paths are obtained for CM-specimens. These experimental results show fairly good agreement with the numerical predictions of the crack path stability made by the proposed theory.

It is found in the present work that the introduction of tapered geometries is not very effective in preventing the sharp crack curving in the fracture specimens. When we use the edge notched fracture specimens of rectangular shape, stable crack paths are expected for the specimens having L/B ratios within the range $L/B < 3.0$.

The validity of the present theory of the crack path stability can be examined by using the experimental results. Here we assume that the stability of the experimentally measured crack paths is represented by the tangent of the crack path $\lambda'(h)$, which can be obtained from the direct measurements. We shall use the following stability criterion;

$$|\lambda'(h)| \begin{cases} < 0.1 : \text{stable} \\ > 0.1 : \text{unstable} . \end{cases} \qquad (15)$$

This criterion corresponds to the sharp crack curving observed in the specimens except for one case experienced in CM-specimen. The experimental results of the crack path stability are shown in the β^*/α- γ^*/α space of Fig.12, in which the previous experimental data [1,3] are also included as well as the present data. As can be seen from Eqn.(14), the relation between γ^*/α and β^*/α becomes parabolic when T/k_I is large compared with other terms. Although we need much more experimental data, the present results seem to indicate that unstable crack paths may occur when both β^*/α and γ^*/α are positive.

ACKNOWLEDGEMENT

This work has been supported by Scientific Research Grant No.5985-0072 from the Ministry of Education to Yokohama National University. Numerical calculations are performed by the computer centers of the University of Tokyo and Yokohama National University.

REFERENCES

[1] Radon,J.C., Leevers,P.S. and Culver,L.E., "Fracture Toughness of PMMA under Biaxial Stress", in Proceedings of ICF4, "Fracture 1977", Edited by D.M.R.Taplin, Vol.3, University of Waterloo Press, Waterloo, Canada, 1977, pp.1113-1118.

[2] Cotterell,B. and Rice,J.R., Int.J. Fracture, Vol.16, No.2, 1980, pp.155-169.

[3] Sumi,Y., Nemat-Nasser,S. and Keer,L.M., Engrg. Fracture Mech., Vol.22, No.5, 1985, pp.759-771.

[4] Sumi,Y., "A Note on the First Order Perturbation Solution of a Straight Crack with Slightly Branched and Curved Extension under a General Geometric and Loading Condition", Engrg. Fracture Mech., in press.

[5] Bueckner,H.F., "Field Singularities and Related Integral Representations", in "Mechanics of Fracture", Edited by G.C.Sih, Vol.1, Noordhoff, Lyden, The Netherlands, 1972, pp.239-314.

[6] Yamamoto,Y. and Tokuda,N., Int.J. Numer. Meth. Engrg., Vol.6, 1973, pp.427-439.

[7] Yamamoto,Y., Tokuda,N. and Sumi,Y., "Accuracy Considerations for Finite Element Calculations of the Stress Intensity Factor by the Method of Superposition", in "Hybrid and Mixed Finite Element Methods", Edited by S.N.Atluri, R.H.Gallagher and O.C.Zienkiewicz, John-Wiley, New York, U.S.A., 1983, pp.361-379.

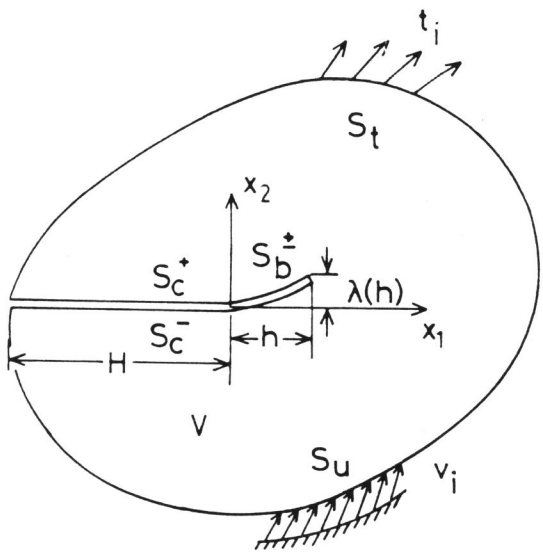

Figure 1 A straight crack with slightly branched and curved extension

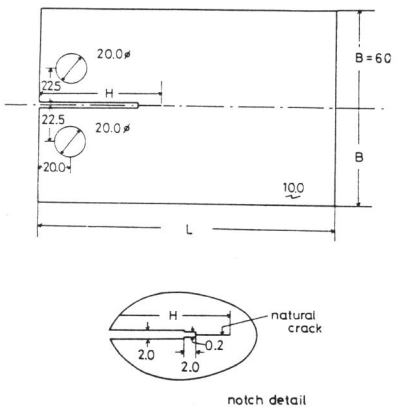

Type A : L=120mm
Type BM: L=180mm
Type BL: L=240mm

Figure 2 Rectangular specimens

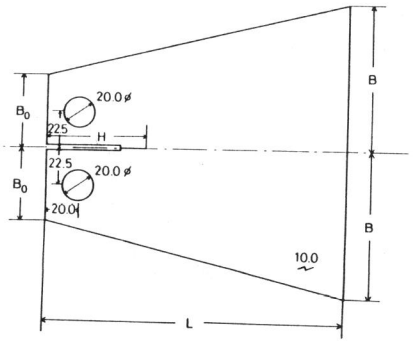

Type CN: L=240mm, B_0=60mm, B=90mm
Type CM: L=240mm, B_0=60mm, B=120mm
Type CW: L=180mm, B_0=45mm, B=112.5mm

Figure 3 Tapered DCB specimens

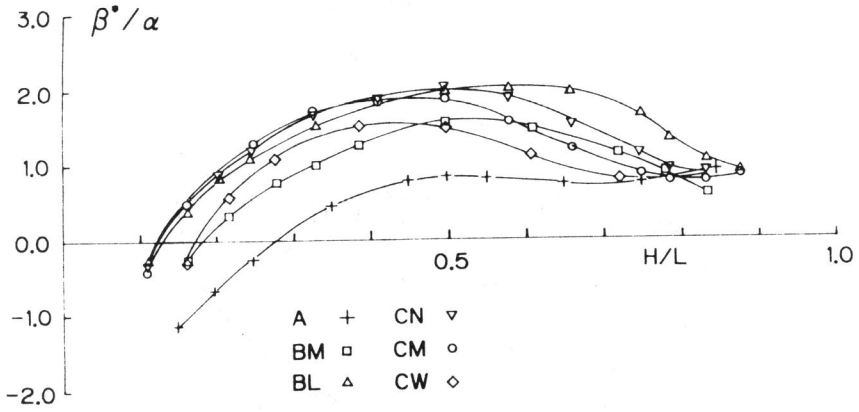

Figure 4 Numerical results of the stability parameter β^*/α for various types of specimens

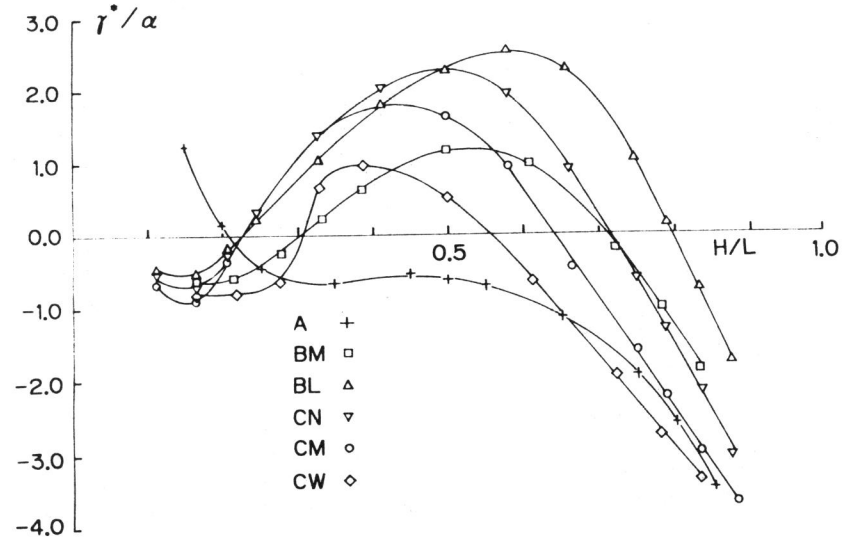

Figure 5 Numerical results of the stability parameter γ^*/α for various types of specimens

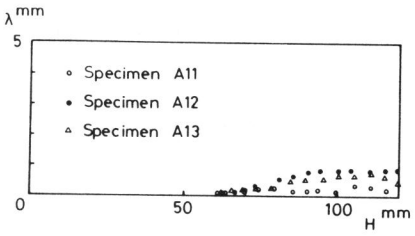

Figure 6 Crack paths of Type-A specimens

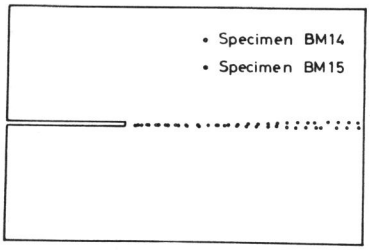

Figure 7 Crack paths of Type-BM specimens

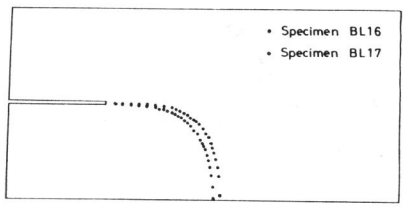

Figure 8 Crack paths of Type-BL specimens

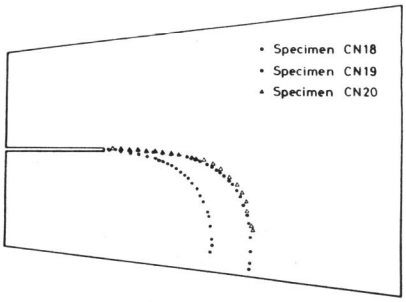

Figure 9 Crack paths of Type-CN specimens

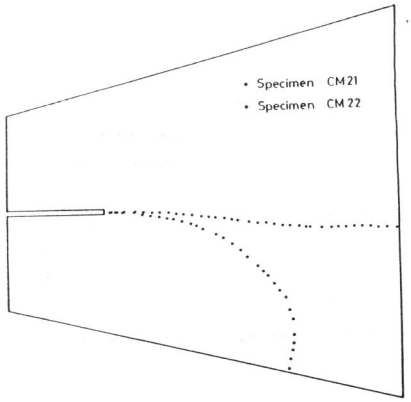

Figure 10 Crack paths of Type-CM specimens

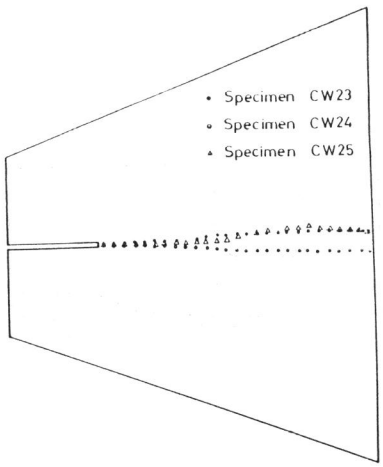

Figure 11 Crack paths of Type-CW specimens

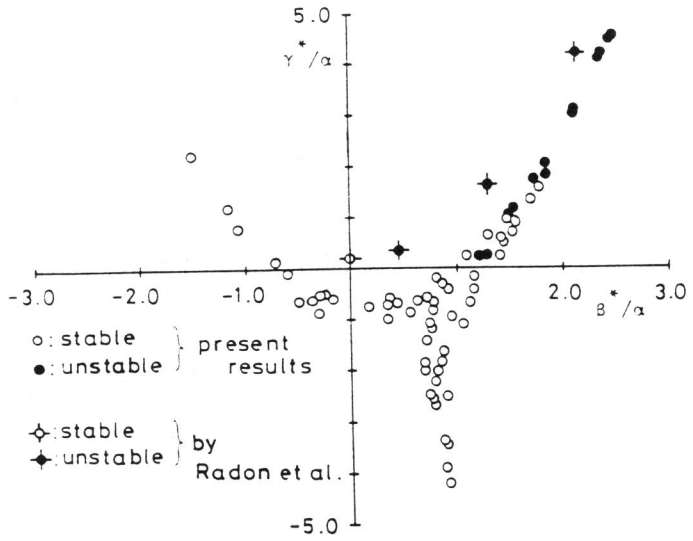

Figure 12 Crack path stability plotted in $\beta^*/\alpha - \gamma^*/\alpha$ plane